
NEURCAM: INTERPRETABLE NEURAL CLUSTERING VIA ADDITIVE MODELS

Nakul Upadhyaya and Eldan Cohen

nakul.upadhyaya@mail.utoronto.ca, ecohen@mie.utoronto.ca
University of Toronto, Toronto, Canada

ABSTRACT

Interpretable clustering algorithms aim to group similar data points while explaining the obtained groups to support knowledge discovery and pattern recognition tasks. While most approaches to interpretable clustering construct clusters using decision trees, the interpretability of trees often deteriorates on complex problems where large trees are required. In this work, we introduce the Neural Clustering Additive Model (NeurCAM), a novel approach to the interpretable clustering problem that leverages neural generalized additive models to provide fuzzy cluster membership with additive explanations of the obtained clusters. To promote sparsity in our model’s explanations, we introduce selection gates that explicitly limit the number of features and pairwise interactions leveraged. Additionally, we demonstrate the capacity of our model to perform text clustering that considers the contextual representation of the texts while providing explanations for the obtained clusters based on uni- or bi-word terms. Extensive experiments show that NeurCAM achieves performance comparable to black-box methods on tabular datasets while remaining interpretable. Additionally, our approach significantly outperforms other interpretable clustering approaches when clustering on text data.

1 Introduction

As Machine Learning (ML) has become more prevalent in society in recent years, the need for trustworthy models that stakeholders can audit has increased dramatically. One desirable aspect of trustworthiness in ML is that the approaches utilized are constrained so that their predictive mechanisms are innately understandable to humans. As a result, they are much easier to troubleshoot and more practical for real-world usage [Rudin, 2019].

One stream of interpretable machine learning is interpretable clustering [Yang et al., 2021]. By using algorithms capable of providing innate explanations of cluster compositions, interpretable clustering methods have found great success in fields such as market segmentation [Aouad et al., 2023], climate science [Sun et al., 2024], and healthcare [Manduchi et al., 2021, Fu et al., 2021]. Most approaches to this task involve the use of decision trees to build clusters [Bertsimas et al., 2021, Fraiman et al., 2013, Frost et al., 2020, Gabidolla and Carreira-Perpiñán, 2022, Shati et al., 2023, Cohen, 2023]. However, the size of decision trees heavily influences their interpretability [Tan et al., 2023, Luštrek et al., 2016], and complex problems may necessitate larger, less interpretable trees.

Another innately interpretable architecture, the Generalized Additive Model (GAM) [Hastie, 2017], has found great success as an interpretable approach in many high-stakes classification and regression tasks [Karatekin et al., 2019, Sarica et al., 2021]. A recent line of work has focused on developing Neural GAMs that enjoy better scalability and are able to learn more expressive, yet interpretable, additive models [Agarwal et al., 2021, Radenovic et al., 2022, Chang et al., 2022, Ibrahim et al., 2024]. Despite these benefits, GAMs have not been utilized for clustering.

In this work, we introduce the **Neural Clustering Additive Model (NeurCAM)**, an interpretable clustering approach that constructs clusters via Neural Generalized Additive Models. Our approach explains how input features influence cluster assignment by modeling the relationship between features and clustering assignments through additive shape functions. Our contributions are as follows:

1. We present a novel approach for interpretable clustering that leverages neural GAMs to provide fuzzy cluster membership. Our approach can leverage deep representations of the data for clustering while still producing explanations in the original feature space. To our knowledge this is the first work to utilize GAMs to provide interpretable clustering.
2. We introduce a mechanism that allows users to explicitly constrain the number of single-feature and pairwise interaction shape functions our model utilizes therefore encouraging sparsity in the final explanations, a key quality of interpretable models [Rudin et al., 2022].
3. Through experimentation on a variety of datasets, we demonstrate NeurCAM’s effectiveness at creating high-quality clusters when using disentangled representations and also showcase the interpretability provided by additive explanations.
4. We demonstrate the capabilities of NeurCAM to perform interpretable text clustering by leveraging transformer-based embeddings in the objective. This allows us to provide uni-word and bi-word explanations while still taking structural and contextual information of the document into account.

The rest of our paper is organized as follows. In Section 2 we outline our desiderata for the interpretable clustering task and discuss prior work that aligns with these objectives. In Section 3 we define GAMs and what makes them interpretable. In Section 4, we describe the components of our approach, NeurCAM, and in Section 5 demonstrate its performance and interpretability.

2 Interpretable Clustering

Our approach for interpretable clustering consists of developing an intrinsically interpretable out-of-sample mapping from samples to clusters. In this section we describe what encompasses this approach, the benefits of achieving it, and discuss existing approaches for interpretable clustering.

2.1 Interpretable Out-of-Sample Mapping

Out-of-Sample Mapping (OSM) in clustering refers to the task of assigning a given sample $\mathbf{x} \in \mathbb{R}^D$ (potentially unseen during training) to a particular cluster using a mapping that is *agnostic of the clustering cost function used* [Gabidolla and Carreira-Perpiñán, 2022]. In particular, OSM allows us to separate the representation of the data used to construct the mapping from samples to clusters from the representation used in the clustering cost function. Previous work has shown that various transformed representations of the original data, such as spectral embeddings, learned embeddings, or PCA, can lead to better clustering performance [Von Luxburg, 2007, Subakti et al., 2022, Chang et al., 2017, Cohen, 2023]. However, such representations are not human-understandable, making it difficult for practitioners to gain insights into the generated clusters. We therefore propose to construct *interpretable* OSM where the mapping is based on interpretable feature representation, while the clustering cost is independently defined over a transformed representation.

2.2 Model-Based Interpretability

We advocate the use of *intrinsically interpretable models* to create the mapping. Formally, our goal is to develop an approach that satisfies the requirements for intrinsic model-based interpretability posed by Murdoch et al. [2019]: *modularity*, *sparsity*, and *simulability*:

- **Modularity:** A ML model can be considered modular if a user can interpret a meaningful portion of its prediction making process independently from other parts of the network [Murdoch et al., 2019].
- **Sparsity:** Sparsity is achieved by limiting the number of non-zero parameters that limit the components a user must analyze to understand model behavior. Understandably, sparse models are easier for practitioners to understand, and hence easier to trust in high-stakes applications [Murdoch et al., 2019, Rudin et al., 2022].
- **Simulability:** An approach is said to be simulable if a human is able to reasonably internally simulate the entire decision-making process [Murdoch et al., 2019]. This requirement synergizes with the prior two requirements, as a model often needs to be sparse and modular for a practitioner to be able to recreate its predictions.

In contrast to model-based interpretability, one may opt to use an uninterpretable model (e.g. deep neural networks) to assign samples to clusters and apply *post hoc* methods to explain clustering decisions. Although useful in many cases, post hoc approaches face a key problem in practice, where users often have to perform analysis on multiple post hoc explanations to identify which method they should trust [Han et al., 2022]. Furthermore, arbitrary post hoc explanations can often be constructed for a given model to obfuscate true biases in the modeling procedure, reducing the trustworthiness of the approach [Slack et al., 2020].

2.3 Existing Approaches

The most prevalent approach to model-based interpretable clustering involves using unsupervised decision trees to partition the space [Bertsimas et al., 2021, Fraiman et al., 2013, Frost et al., 2020, Shati et al., 2023, Cohen, 2023, Gabidolla and Carreira-Perpiñán, 2022]. The most relevant approaches to our work are the soft clustering tree (SCT) [Cohen, 2023] and the tree-alternating optimization (TAO) clustering [Gabidolla and Carreira-Perpiñán, 2022]. Both approaches utilize a decision tree to map points to clusters and support OSM with separate representations. The SCT utilizes an axis-aligned soft-decision tree trained through continuous optimization methods (including mini-batch gradient descent) [Cohen, 2023], while TAO iteratively refines a tree that approximates a K-means clustering via alternating optimization [Gabidolla and Carreira-Perpiñán, 2022].

Despite their interpretable nature, tree-based approaches face a substantial interpretability-performance trade-off as complex problems require large trees to represent cluster boundaries adequately, reducing the sparsity of these approaches. Growing the number of leaves in a tree has been shown to significantly increase the difficulty users face when trying to understand the decision pathways of the model [Luštrek et al., 2016]. Furthermore, increasing the number of features used in the decision tree significantly increases the time it takes users to analyze the tree and understand what features are essential for predictions [Tan et al., 2023].

Other interpretable clustering approaches include the construction of clusters using polytope machines [Lawless et al., 2022] and rectangular rules [Chen et al., 2016].

Some notable post-hoc approaches include Kauffmann et al. [2022] who explains a neural clustering via layerwise relevance propagation [Bach et al., 2015], Lawless and Gunluk [2023] who profiles assignments via Polyhedral Descriptions, and Carrizosa et al. [2022] who profiles assignments via prototypical examples. Additionally, Guan et al. [2020] proposed to cluster text using deep embeddings and then performed a post hoc approximation of the clustering via a logistic regression on a bag-of-words representation. TELL [Peng et al., 2022] and IDC [Svirsky and Lindenbaum, 2024] both cluster via a layer in a Neural Network. Similar to post hoc methods, these approaches do not satisfy our desiderata for model-based interpretability (Section 2.2).

3 Generalized Additive Models

In this work, we propose to construct an interpretable cluster map using a Generalized Additive Model. Given a D -dimensional input $\mathbf{x} = \{x_i\}_{i=1}^D$, $\mathbf{x} \in \mathbb{R}^D$, univariate shape functions f_i corresponding to the input features x_i , bivariate shape functions f_{ij} corresponding to the features x_i and x_j , and link function $g(\cdot) : \mathbb{R}^D \rightarrow \mathbb{R}$, the predictions of a GAM and GA²M are defined as follows:

$$\text{GAM} : g(\mathbf{x}) = f_0 + \sum_{i=1}^D f_i(x_i) \quad (1)$$

$$\text{GA}^2\text{M} : g(\mathbf{x}) = f_0 + \sum_{i=1}^D \left(f_i(x_i) + \sum_{j>i}^D f_{ij}(x_i, x_j) \right) \quad (2)$$

In recent years, many powerful GAM models have been proposed, the primary difference between them being how shape functions are constructed. Some notable examples include the Explainable Boosting Machine [Lou et al., 2013a], which uses tree ensembles trained using a cyclical gradient boosting algorithm, and NODE-GAM [Chang et al., 2022], which leverages layers of ensemble oblivious neural decision trees.

Additionally, many works have proposed representing the shape function of the GAMs through MLPs such as Neural Additive Models (NAM) [Agarwal et al., 2021], which trains an MLP for each feature, and Neural Basis Models [Radenovic et al., 2022] which extend NAM by constraining all features to utilize a common MLP backbone except for the last layer, which is unique to each feature.

Interpretability of GAMs GAM and GA²M satisfy the model-based interpretability requirements previously posed. GAMs force the relationship between the features in the model to be additive, resulting in a *modular* model [Murdoch et al., 2019]. This modularity allows the contribution of each feature or interaction to the prediction to be visualized as a graph or heatmap, allowing humans to *simulate* how a GAM works by querying the different graphs and adding the results together [Lou et al., 2013b, Chang et al., 2021]. This enables decision makers in high-stakes fields such as healthcare to easily understand the explanations provided by GAM and GA²M shape functions [Hegselmann et al., 2020, Agarwal et al., 2021]. Technical stakeholders have also shown a preference for GAMs over post hoc explanations such as SHAP values [Lundberg and Lee, 2017], as they reduce the cognitive load needed to grasp a

model’s decision mechanisms, enhancing stakeholders’ confidence in the deployed ML system [Kaur et al., 2020]. Furthermore, stakeholders have shown a preference for additive explanations over tree explanations when both utilize a similar number of features [Tan et al., 2023]. To further ensure that the explanations provided by NeurCAM are *sparse*, we propose selection gates that allow users to enforce a cardinality constraint on the number of features and interactions used.

4 NeurCAM

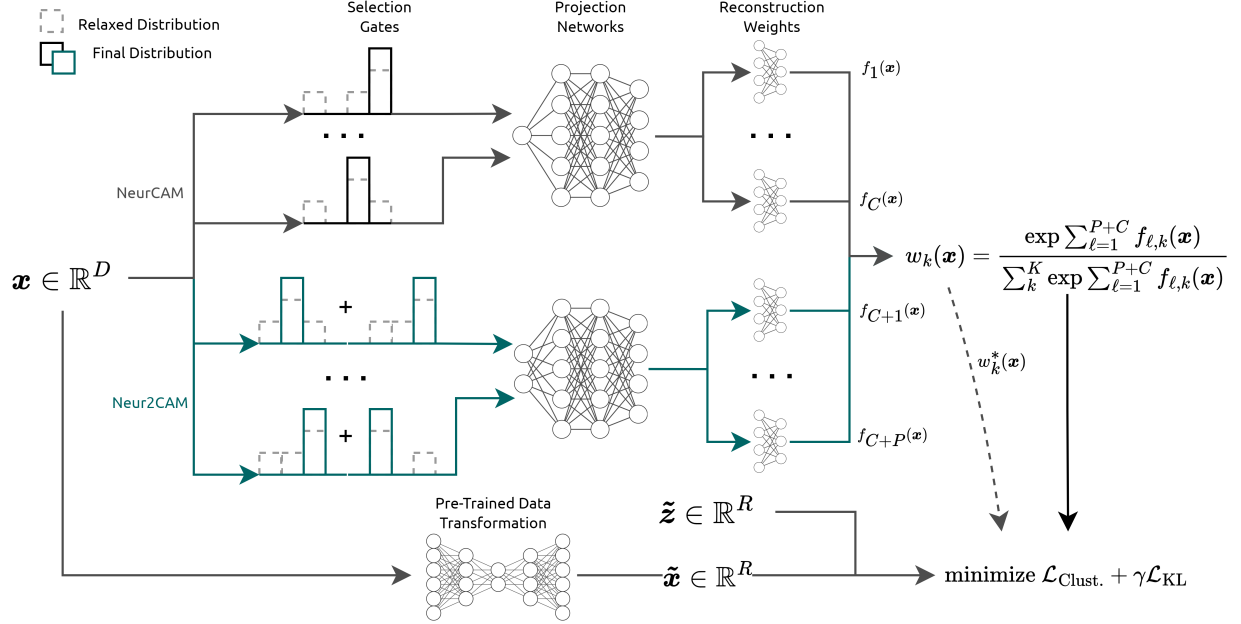


Figure 1: Our proposed approach. We leverage multiple shape functions that each pick a feature via a selection gate. The final prediction is the sum of the individual shape function contributions. The black shape functions represents NeurCAM and the additional blue pairwise shape functions represent Neur2CAM.

In this work, we consider the following problem: Let $X = \{\mathbf{x}_n\}_{n=1}^N$ be a set of N data points with \mathbf{x}_n being a D -dimensional feature vector $\mathbf{x}_n \in \mathbb{R}^D$. We aim to decide fuzzy cluster assignments $w_{n,k} \in [0, 1]$, $\sum_k w_{n,k} = 1.0$ for each point \mathbf{x}_n and cluster $k \in 1, 2, \dots, K$. Our approach to this problem involves utilizing a Neural GAM to obtain the assignments (Section 4.1) and train this GAM through a combination of a fuzzy clustering loss and self-supervised regularization (Section 4.2).

4.1 Model Architecture

In the following section, we describe how we obtain the cluster assignments via an interpretable neural GAM. For succinctness, we drop the sample index n in this section.

4.1.1 Neural Basis Model

For our additive model, we leverage a Neural Basis Model (NBM) [Radenovic et al., 2022] which we describe here for thoroughness.

The NBM operates by projecting each feature $x_i, i = 1, 2, \dots, D$ onto B basis functions that are shared between all features. The projection function $\mathbf{b}(\cdot) : \mathbb{R} \rightarrow \mathbb{R}^B$ is represented by an MLP backbone with a single input and B outputs. The projection of each feature is then reconstructed into the final shape function for each cluster via a linear combination, with each feature having its own set of weights for each cluster $\lambda_{i,k} \in \mathbb{R}^B$. More concretely, the prediction from a single feature x_i is as follows:

$$\mathbf{b}(x_i) = \text{MLP}(x_i) \quad (3)$$

$$f_{i,k}(\mathbf{x}) = \lambda_{i,k} \cdot \mathbf{b}(x_i) \quad (4)$$

The resultant logits assigned to each cluster $h_k(\mathbf{x})$, $k = 1, 2, \dots, K$ is the sum of the contributions from each feature:

$$g_k(\mathbf{x}) = \sum_i^D f_{i,k}(\mathbf{x}) \quad (5)$$

These logits are transformed via the softmax operation to obtain the final fuzzy assignment weights:

$$w_k(\mathbf{x}_n) = \frac{\exp(g_k(\mathbf{x}))}{\sum_{k'=1}^K \exp(g_{k'}(\mathbf{x}))} \quad (6)$$

Pairwise interaction can be represented in a similar manner using an MLP with two inputs instead of one.

4.1.2 Feature Selection Gates

A common problem across MLP-based GAMs and GA²Ms is the variable explosion problem. As the dimensionality of the dataset increases, the number of single-feature and pairwise shape functions rapidly increases as well. This is especially true for GA²Ms as the number of pairwise interactions grows quadratically with the dimensionality of the dataset. Previous MLP-based approaches have no inherent mechanisms to limit pairwise interactions and instead utilize heuristics based on residual analysis of a fitted GAM to select interactions to use in the GA²M [Agarwal et al., 2021, Radenovic et al., 2022]. However, this approach does not translate to the unsupervised setting as there are no residuals due to the absence of true labels.

Instead, we propose to *learn* what features and interactions are in our model through feature selection gates. More concretely, NeurCAM learns C independent shape functions. The feature used by shape function $c \in 1, \dots, C$ is selected via a selection function $s_c(\mathbf{x}) : \mathbb{R}^D \rightarrow \mathbb{R}$. A common way to represent such a function is the product of the feature vector and a one-hot selection vector \mathbf{F}_c where a variable is selected if its corresponding selection logit $\tilde{F}_c \in \mathbb{R}^D$ is the largest:

$$s_c(\mathbf{x}) = \mathbf{F}_c \cdot \mathbf{x} \quad (7)$$

$$F_{c,i} = \begin{cases} 1 & i = \text{argmax}(\tilde{F}_c) \\ 0 & \text{else} \end{cases} \quad (8)$$

To train this selection as part of our network, we *temporarily* relax the one-hot vector to be represented by entmax _{α} [Peters et al., 2019], a sparse version of softmax that allows elements to become exactly zero if the logits are sufficiently small:

$$s_c(\mathbf{x}) = \text{entmax}_\alpha(\tilde{F}_c/T) \cdot \mathbf{x} \quad (9)$$

Here, $T > 0$ is a temperature annealing parameter that controls the sparsity of the distributions obtained from the entmax _{α} operations, with smaller values of T resulting in sparser distributions. As $T \rightarrow 0$, the resultant distribution will become one-hot.

At the start of training, we set $T = 1.0$, making the gate a weighted mixture of features. After a number of warm-up training epochs, we anneal T by a factor of $\epsilon \in (0, 1)$ until $\text{entmax}_\alpha(\tilde{F}_c/T) \cdot \mathbf{x} = x_{\text{argmax}(\tilde{F}_c)}$, allowing $s_c(\cdot)$ to serve as a proper feature selection gate and making NeurCAM a valid GAM once again. The factor ϵ is a hyperparameter that controls how gradual the tempering is, with higher epsilon values resulting in a slower annealing process and lower values resulting in a faster annealing.

We modify the NBM to include these selection gates to obtain the additive model architecture used by NeurCAM whos prediction mechanisms are as follows:

$$\mathbf{b}(\mathbf{x}) = \text{MLP}(s_c(\mathbf{x})) \quad (10)$$

$$f_{c,k}(\mathbf{x}) = \lambda_{c,k} \cdot \mathbf{b}(\mathbf{x}) \quad (11)$$

$$g_k(\mathbf{x}) = \sum_{c=1}^C f_{c,k}(\mathbf{x}) \quad (12)$$

A softmax is then applied to $g_1(\mathbf{x}), g_2(\mathbf{x}) \dots, g_K(\mathbf{x})$ to obtain the soft cluster assignments $\mathbf{w}(\mathbf{x})$ like in Equation (6).

The number of shape functions serves as an upper bound for the number of features utilized by the model, and the features used in the model’s explanations can be limited by setting $C < D$. The choice of C is problem and stakeholder specific.

While we apply this mechanism on an NBM, these selection gates can be applied to other Neural GAM models such as the Neural Additive Model [Agarwal et al., 2021].

Extending to Neur2CAM: To extend NeurCAM to allow pairwise interactions, we introduce P additional shape functions whose selection gates allow for two features. More concretely, the pairwise interaction used by shape function $p \in C + 1, \dots, C + P$ is chosen by selection function $s_p^2(\mathbf{x}) : \mathbb{R}^D \rightarrow \mathbb{R}^2$, defined as:

$$s_p^2(\mathbf{x}) = \begin{bmatrix} \text{entmax}_\alpha(\tilde{\mathbf{F}}_{p,0}/T_2) \\ \text{entmax}_\alpha(\tilde{\mathbf{F}}_{p,1}/T_2) \end{bmatrix} \mathbf{x} \quad (13)$$

Like the single-order case, the pairwise temperature annealing parameter T_2 is set to 1.0 during the warmup phase and is annealed to near zero afterwards. All pairwise shape function share a common two-input MLP backbone that projects a pair of features into B outputs, with each shape function having its own set of reconstruction weights used to build the final shape functions. In theory, our approach can extend NeurCAM to interactions of any order, but we only explore up to pairwise to maintain a high degree of interpretability.

4.2 Training NeurCAM

In this section we describe the loss function and procedure used to train NeurCAM.

4.2.1 Fuzzy Clustering Loss

We employ a loss function inspired by Fuzzy C-Means [Bezdek et al., 1984]:

$$\mathcal{L}_{\text{Clust}} = \sum_{n=1}^N \sum_{k=1}^K w_k(\mathbf{x}_n)^m \|\mathbf{x}_n - \mathbf{z}_k\|^2 \quad (14)$$

Here $m \geq 1.0$ is a hyperparameter controlling the fuzziness of the clustering. Our loss departs from Fuzzy C-Means in two main ways. In contrast to Fuzzy C-Means where the cluster assignment weights are free variables, our assignment weights are parameterized by an interpretable GAM (Equation (6)).

Additionally, instead of the centroids of the clusters being calculated by the clustering assignments [Bezdek et al., 1984], we opt to make the centroids $\mathbf{z}_k \in \mathbb{R}^D, k = 1, \dots, K$ free variables to aid in the optimization of our network.

4.2.2 Disentangling Representations

The mapping constructed by NeurCAM is agnostic to how the distance between samples and the cluster centroids are defined. As such, we decouple the representations of the data in our loss function into the interpretable representation \mathbf{x} and the transformed representation $\tilde{\mathbf{x}} \in \mathbb{R}^R$.

NeurCAM maps a sample to a given cluster using the interpretable feature set. However, the distance from each sample to the centroids of the clusters will be calculated using the transformed representation:

$$\mathcal{L}_{\text{Clust}} = \sum_{n=1}^N \sum_{k=1}^K w_k(\mathbf{x}_n)^m \|\tilde{\mathbf{x}}_n - \tilde{\mathbf{z}}_k\|^2 \quad (15)$$

It is important to note that the learned centroids $\tilde{\mathbf{z}}_k \in \mathbb{R}^R$ are in the same space as the transformed representation $\tilde{\mathbf{x}}$.

4.2.3 Self-Supervised Regularization

Empirically, we observe that while our model is able to achieve a high-quality clustering at the end of the warm-up period, the selection gate annealing process often significantly degrades the ability of our network to directly optimize the clustering loss (Equation (15)) and can lead to poor local optima. To mitigate this degradation, we propose to take advantage of the clustering discovered at the end of the warm-up period, denoted by $\mathbf{w}^*(\mathbf{x}_n) \in \mathbb{R}^K$, to guide the optimization process after the annealing process starts.

When we start annealing the selection gates' temperatures T and T_2 toward zero, we add a regularization term that penalizes the KL-divergence between the current mapping $\mathbf{w}(\mathbf{x}_n)$ and the mapping $\mathbf{w}^*(\mathbf{x}_n)$ discovered at the end of the warm-up phase.

$$\mathcal{L}_{\text{KL}} = \sum_{n=1}^N \sum_{k=1}^K w_k^*(\mathbf{x}_n) \log \frac{w_k^*(\mathbf{x}_n)}{w_k(\mathbf{x}_n)} \quad (16)$$

The final objective utilized after the warmup phase is as follows:

$$\text{minimize } \mathcal{L}_{\text{Clust}} + \gamma \mathcal{L}_{\text{KL}} \quad (17)$$

Where γ is a parameter that controls the weight of the KL term. The complete pseudocode of NeurCAM’s training procedure can be found in Algorithm (1).

Algorithm 1: NeurCAM Training Pseudocode

Input: $X, \tilde{X}, K, \gamma, \alpha, \epsilon, E_{\text{warmup}}, E_{\text{total}}$
 $\tilde{z} \leftarrow \text{InitializeCentroids}(\tilde{X})$
 $\theta_{\text{GAM}} \leftarrow \text{RandomInitModelParams}()$
 $\theta \leftarrow \tilde{z} \cup \theta_{\text{GAM}}$
 $T \leftarrow 1.0$
for $E = 1, 2, \dots, E_{\text{total}}$ **do**
 if $E = E_{\text{warmup}}$ **then**
 $\theta^* \leftarrow \theta$
 end
 for $(X_{\text{batch}}, \tilde{X}_{\text{batch}}) \in (X, \tilde{X})$ **do**
 $w_{\text{batch}} \leftarrow \text{ForwardPass}(X_{\text{batch}}, \theta, T)$
 if $E > E_{\text{warmup}}$ **then**
 $w_{\text{batch}}^* \leftarrow \text{ForwardPass}(X_{\text{batch}}, \theta^*, 1.0)$ $\mathcal{L}_{\text{KL}} \leftarrow \text{KL}(w_{\text{batch}}^* || w_{\text{batch}})$
 else
 $\mathcal{L}_{\text{KL}} \leftarrow 0$
 end
 $\mathcal{L}_{\text{Clust}} \leftarrow \text{CalculateClustLoss}(\tilde{X}_{\text{batch}}, w_{\text{batch}}, \tilde{z})$
 $\mathcal{L} \leftarrow \mathcal{L}_{\text{Clust}} + \gamma \mathcal{L}_{\text{KL}}$
 $\theta \leftarrow \theta - \alpha \nabla \mathcal{L}$
 end
 if $\exists c \ s_c(x) \neq x_{\text{argmax}(\tilde{F}_c)}$ **then**
 $T \leftarrow \epsilon T$
 end
end

5 Experiments and Evaluation

In this section, we highlight the benefits of our approach in various real-world datasets. We first demonstrate our ability to generate high-quality clusters using disentangled representations on tabular data sets. We later extend our approach to text clustering. In addition, we validate our training scheme via an ablation study and provide an analysis of the interpretability of NeurCAM.

5.1 Experimental Details

We run experiments with two variants of our approach. NeurCAM (NCAM) includes only single-feature shape functions, and Neur2CAM (N2CAM), which extends NeurCAM to include pairwise interaction.

For our interpretable benchmarks, we consider approaches that provide model-based interpretability and are capable of disentangling representations, namely the recently proposed Soft Clustering Trees (SCT) [Cohen, 2023] and the axis-aligned TAO Clustering Tree (TAO) [Gabidolla and Carreira-Perpiñán, 2022]. For both of these tree-based approaches, we consider two different depths. We first consider a highly interpretable shallow tree with a depth of five (SCT/TAO-5). This choice also guarantees that the number of leaves is greater than the number of clusters across all datasets. For a more expressive, but less sparse, baseline, we also consider trees with a depth of seven (SCT/TAO-7). As a representative of black-box clustering methods, we compare with Mini-Batch K -Means (mKMC) [Sculley, 2010], a scalable variant of K-Means.

Evaluation Metrics As all of our utilized datasets come with known labels, we assess the clustering results using three external evaluation measures: Adjusted Rand Index (ARI), Normalized Mutual Information (NMI), and Unsupervised Clustering Accuracy (ACC). We also report the Inertia (Iner.) normalized by the number of datapoints in the dataset.

For our fuzzy models (NeurCAM and SCT), we calculate all metrics using the hard clustering decision obtained by selecting the cluster with the highest fuzzy weight for each data point at inference time.

Rand index (RI) [Rand, 1971] measures agreements between two partitions of the same dataset P_1 and P_2 with each partition representing $\binom{n}{2}$ decisions over all pairs, assigning them to the same or different clusters and is defined as follows:

$$\text{RI}(P_1, P_2) = \frac{a + b}{\binom{n}{2}} \quad (18)$$

Where a is the number of pairs assigned to the same cluster, and b is the number of pairs assigned to different clusters. ARI [Hubert and Arabie, 1985] is a correction for RI based on its expected value:

$$\text{ARI} = \frac{\text{RI} - \mathbb{E}(\text{RI})}{\max(\text{RI}) - \mathbb{E}(\text{RI})} \quad (19)$$

An ARI score of zero indicates that the cluster assignment is no better than a random assignment, while a score of 1 indicates a perfect match between the two partitions.

Normalized Mutual Information measures the statistical information shared between distributions [Strehl and Ghosh, 2002], normalized by the average entropy of the two distributions. This metric is defined as follows:

$$\text{NMI}(P_1, P_2) = \frac{\text{MI}(P_1, P_2)}{\text{mean}(H(P_1), H(P_2))} \quad (20)$$

Where $H(\cdot)$ is the entropy of a given distribution and $\text{MI}(P_1, P_2)$ is the mutual information between P_1 and P_2 .

Unsupervised clustering accuracy [Xie et al., 2016] measures the best agreement between the cluster label c_n and the ground-truth l_n .

$$\text{ACC} = \max_{\text{map} \in M} \frac{1}{N} \sum_{n=1}^N \mathbb{1}\{l_n = \text{map}(c_n)\} \quad (21)$$

M is the set of all possible one-to-one mappings from clusters to ground-truth labels.

Inertia is defined as the sum of the squared distances from the representation of the datapoints and the centroids of the cluster they are assigned to:

$$\text{Inertia} = \sum_{n=1}^N \sum_{k=1}^K w_{n,k} \|\tilde{\mathbf{x}}_n - \mathbf{z}_k\|^2 \quad (22)$$

$$w_{n,k} \in \{0, 1\}, \sum_{k=1}^K w_{n,k} = 1 \quad \forall n = 1, 2, \dots, N \quad (23)$$

Training and Implementation Details All models and benchmarks are implemented in Python. The SCT and NeurCAM are implemented in PyTorch [Paszke et al., 2019] and we utilize the Mini-Batch K -Means implementation found in the Scikit-Learn package [Pedregosa et al., 2011]. For TAO, the implementation from the original paper is not publicly available and we implemented the approach following the details outlined by Gabidolla and Carreira-Perpiñán [2022].

NeurCAM is trained using the Adam [Kingma and Ba, 2014] optimizer with plateau learning rate decay. For Neur2CAM, the pairwise gate temperature parameter T_2 is fully annealed before T starts its annealing procedure. To initialize the centroids $\tilde{\mathbf{z}}$, we utilize centroids obtained from Mini-Batch K -Means clustering. Training details and hyperparameters for NeurCAM and the other approaches can be found in Appendix C.

As our model and all benchmarks may converge to a locally optimum solution, we perform five runs with different random seeds and select the run with the lowest Inertia value for the hard clustering.

Extracting Shape Graphs: To extract the final shape graphs for each feature and interaction in NeurCAM, we query the predictions from each individual shape function and then combine the shape functions that have selected the same feature (or interaction) to obtain the final shape graphs:

$$f_{i,k}(\mathbf{x}) = \sum_{c=1}^C \mathbb{1}_i(\mathbf{F}_c) f_{c,k}(\mathbf{x}) \quad (24)$$

$$f_{i,j,k}(\mathbf{x}) = \sum_{p=C+1}^{C+P} \mathbb{1}_{i,j}(\mathbf{F}_{p,0}, \mathbf{F}_{p,1}) f_{p,k}(\mathbf{x}) \quad (25)$$

Here $\mathbb{1}_i(\cdot)$ is an indicator function on whether feature i is selected and $\mathbb{1}_{i,j}(\cdot, \cdot)$ is an indicator function on whether both features i and j were selected in the selection vectors (regardless of the order). Following Agarwal et al. [2021] and Radenovic et al. [2022], we set the average cluster activation (logits) of each feature’s shape function to zero by subtracting the mean activation. For the pairwise shape graphs of Neur2CAM, we adopt GA²M purification to push interaction effects into main effects if possible [Lengerich et al., 2020]. To derive feature-importance from our model, we follow Lou et al. [2013a] and take the average absolute area under the shape graph.

5.2 Clustering Tabular Data

We demonstrate the ability of our model to create high-quality cluster assignments on tabular tasks by testing it on six datasets from the UCI repository [Kelly et al., 2017]: Adult, Avila, Gas Drift, Letters, Pendigits, and Shuttle. All datasets were standardized by removing the mean and scaling to unit variance. Information about these datasets can be found in Appendix B.

In this set of experiments we set the number of single-feature shape functions equal to the number of features. For Neur2CAM, we set the number of pairwise shape functions equal to the number of single-feature shape functions to maintain a high degree of interpretability. We set $m = 1.05$ for our loss function (Equation (15)).

Representations Utilized: For our interpretable representation x , we utilize the original feature space provided by the datasets. For the representation in our loss function \tilde{x} , we consider two different deep transformations:

- Denoising AutoEncoder (DAE): We cluster on the embeddings from a pre-trained DAE [Vincent et al., 2008] with dropout corruption and a bottleneck of size 8.
- SpectralNet (Spectral): We cluster on embeddings from a SpectralNet [Shaham et al., 2018], a deep-learning based approximation of Spectral Clustering [Von Luxburg, 2007]. The embedding dimension is equal to the number of clusters in the dataset.

NeurCAM, the SCT, and TAO make clustering decisions using the original, interpretable feature space, while Mini-Batch K -Means directly clusters in the transformed space.

5.2.1 Results

Table 1: Summarized results from our tabular clustering experiments. The best overall results are highlighted in bold, while the best interpretable results are underlined. The dashed line separates interpretable and non-interpretable approaches.

		ARI		NMI		ACC		Iner.	
		AE	Spectral	AE	Spectral	AE	Spectral	AE	Spectral
Average Scores	NCAM	0.192	0.261	0.303	0.385	0.524	0.561	2.509	1.995
	N2CAM	0.190	0.272	0.295	0.394	0.517	0.568	2.399	1.994
	TAO-5	0.185	<u>0.240</u>	0.287	<u>0.347</u>	0.521	<u>0.515</u>	2.960	<u>4.181</u>
	TAO-7	0.189	0.257	0.291	0.371	0.526	0.518	2.315	2.517
	SCT-5	0.159	0.190	0.276	0.314	0.452	0.479	3.552	5.460
	SCT-7	0.157	<u>0.198</u>	0.267	0.315	0.469	0.476	3.416	4.443
	mKMC	0.211	0.250	0.301	0.380	0.512	0.520	2.682	1.579
Average Rank	NCAM	9.50	4.17	8.17	3.33	7.00	4.67	2.83	3.17
	N2CAM	8.83	3.00	7.83	3.00	7.67	3.50	2.67	<u>3.50</u>
	TAO-5	9.67	<u>6.50</u>	9.50	5.83	6.83	7.83	4.67	4.50
	TAO-7	9.50	5.67	9.50	4.33	7.00	7.00	3.00	3.17
	SCT-5	9.83	6.00	10.83	6.33	9.83	9.50	6.50	6.50
	SCT-7	11.33	<u>8.50</u>	12.00	7.33	10.17	9.67	5.83	5.33
	mKMC	7.00	4.00	8.17	3.33	7.33	6.00	2.33	1.67

Table 1 provides a summary of the comparison between our approach and our baselines on the tabular data sets. A detailed breakdown of the results by dataset can be found in Appendix D.

We observe that our approaches on SpectralNet embeddings consistently outperforms baselines in average rank on external metrics across all datasets. This trend remains consistent when looking at the average value across data sets, as well.

When considering Inertia for SpectralNet embeddings, we achieve the best average value and average rank across the interpretable methods. Although TAO-7 is able to obtain a slightly lower Inertia value on DAE embeddings, we still achieve a lower average rank, indicating that our approaches result in lower Inertia more often.

5.3 Clustering Text Data

Table 2: Summarized results from our text clustering experiments. The best overall results are highlighted in bold, while the best interpretable results are underlined. The dashed line separates interpretable and non-interpretable approaches.

		ARI \uparrow	NMI \uparrow	ACC \uparrow	Iner. \downarrow
Average Values	NCAM	0.359	0.463	0.584	696.717
	N2CAM	<u>0.455</u>	<u>0.546</u>	<u>0.625</u>	<u>686.311</u>
	TAO-5	0.052	0.236	0.286	737.509
	TAO-7	0.081	0.272	0.346	730.358
	SCT-5	0.127	0.233	0.333	738.614
	SCT-7	0.134	0.224	0.320	737.754
	mKMC	0.491	0.570	0.659	674.071
Average Rank	NCAM	3.00	3.00	2.75	3.0
	N2CAM	1.75	1.50	2.00	2.0
	TAO-5	<u>6.25</u>	<u>6.00</u>	<u>6.00</u>	<u>6.0</u>
	TAO-7	5.25	4.75	4.75	4.5
	SCT-5	5.50	5.00	5.50	6.0
	SCT-7	5.00	6.25	5.75	5.5
	mKMC	1.25	1.50	1.25	1.0

Our approach can be utilized for any task where a human-understandable tabular representation can be extracted. We demonstrate this ability by extending our approach to perform text clustering on 4 text datasets: AG News [Zhang et al., 2015], DBPedia [Auer et al., 2007], 20 Newsgroups [Lang, 1995], and Yahoo Answers [Zhang et al., 2015]. For AG News, DBPedia, and Yahoo, we follow the approach taken in the previous literature [Subakti et al., 2022, Wang et al., 2016] and sample 1,000 points from each class.

To create our interpretable representation, we remove the punctuation, lowercase, and tokenize all datapoints. We then lemmatize all tokens using the WordNet [Miller, 1995] lemmatizer available in the Natural Language Toolkit (NLTK) [Bird et al., 2009] and remove english stopwords, corpus-specific stopwords that appear in more than 99% of the datapoints, and rare words that appear in less than 1% of the documents. Finally, we then calculate term-frequency in each datapoint and normalize the representation so that the L_2 norm of the resultant vector is equal to 1.0.

For the representation in our loss function (Equation (15)), we leverage embeddings from the MPNet pretrained transformer [Song et al., 2020] available in the Sentence Transformers package [Reimers and Gurevych, 2019]. This model has a representation size of 768, a maximum sequence length of 384, and uses mean pooling to construct its embedding.

To retain model sparsity, we opt to only use 128 single feature shape functions and 128 pairwise shape functions (when applicable). We set $m = 1.025$ for our loss function (Equation (15)).¹

5.3.1 Results

Table 2 provides a summary of the comparison between our approaches and our baselines on the text datasets. A detailed breakdown of the results by dataset can be found in Appendix E.

We observe that our approaches significantly outperform the interpretable baselines. Neur2CAM and NeurCAM obtain the first and second place, respectively, when considering the interpretable models across both external and internal metrics in both average value and average rank. More concretely, NeurCAM has a 167.9% higher ARI than the SCT of depth seven and a 4.6% lower Inertia than TAO with depth seven. The introduction of pairwise interactions makes this gap even more drastic, with Neur2CAM having both a higher average ARI (26. 6% higher) and a lower average Inertia (1.5% lower) than NeurCAM.

¹On the text datasets, we empirically observed that $m = 1.05$ resulted in degenerate solutions, therefore a smaller m value was used.

As expected, given the restrictions we imposed on our feature space, our interpretable approaches do not outperform the black-box model. However, despite significantly limiting the number of terms and interactions used,² we were able to obtain more than 92% of the performance of the black-box model (Mini-Batch K -Means) across all external evaluation metrics. More specifically, Neur2CAM achieves an ARI equal to 92.7% of the ARI, 95. 9% of the NMI and 94. 8% of the ACC achieved by Mini-Batch K -Means. Furthermore, Neur2CAM achieves an average Inertia value within 1.8% of Mini-Batch K -Means.

5.4 Ablation Analysis

Table 3: Results of our ablation analysis. Full is our approach with both terms in the loss function. No CL denotes ablating the clustering loss term and No KL denotes ablating the KL-Divergence term.

		NeurCAM		Neur2CAM	
		Loss	Iner.	Loss	Iner.
Average	Full	83.454	696.717	82.646	686.311
	No CL	84.254	698.432	83.012	686.824
	No KL	83.568	702.358	83.031	691.754

To demonstrate the benefit of the loss terms used in the second phase of our training, we introduce two ablations of NeurCAM. The first ablation removes the clustering loss (Equation (15)) in the second phase of training, making NeurCAM to optimize only the KL divergence between NeurCAM and its relaxation. The second ablation keeps the clustering loss term, but instead ablates the KL-Divergence loss (Equation (16)) so that NeurCAM only optimizes the clustering loss throughout its training. We perform this analysis on our text datasets and report both the loss (Equation (15)) and the Inertia of the run that achieves the minimum Inertia across five seeds. We observe that including both terms in our loss function consistently results in lower values across both metrics.

5.5 Interpretability of NeurCAM

In this section, we highlight the interpretability of NeurCAM and connect it back to the model-based interpretability desiderata presented in Section 2.2.

5.5.1 Controllable Sparsity

NeurCAM allows users to explicitly control the number of features and interactions used to construct the clusters through our selection gate mechanism (Equations (9) and (13)). In many cases, users can significantly limit the number of shape functions used, improving the model sparsity while still generating high-quality clusters. To demonstrate this capability, we ablate the number of selection gates utilized. We report the ratio between the Inertia of Neur2CAM (minimum across five random seeds) and the Inertia of Mini-Batch K -Means (also across five random seeds) and plot the cost ratio as we vary the number of pairwise shape functions. To isolate the impact of using interactions, we set the number of single feature shape functions to zero for this experiment. In Figure 2, we observe that we are able to achieve a loss value comparable to Mini-Batch K -Means with only 4 shape functions, or at most 4 pairwise interactions, when clustering on both the Pendigits and Letters dataset.

5.5.2 Modularity and Simulability

The learned shape functions for each feature and interaction in NeurCAM are *modular* and can be independently analyzed, allowing stakeholders to understand the impact individual features have on the end prediction as well as *simulate* predictions by querying the different shape functions. As an example, Figure 3 we displays the shape function learned by NeurCAM when clustering the AG News Text Dataset for the term “Microsoft”. When examining this shape graph, we can see that when Microsoft is present in a sample, the network allocates more weight to Cluster 4 and reduces the weight to the other clusters. When examining the alignment between the clusters and the ground-truth labels, we observed that cluster 4 consists primarily of news titles related to technology, indicating that the presence of Microsoft in a sample results in NeurCAM mapping the sample to the “technology” cluster. A full example of NeurCAM’s explanations can be found in Appendix H.

²We use a maximum of 128 interactions out more than 50,000 possible pairwise interactions.

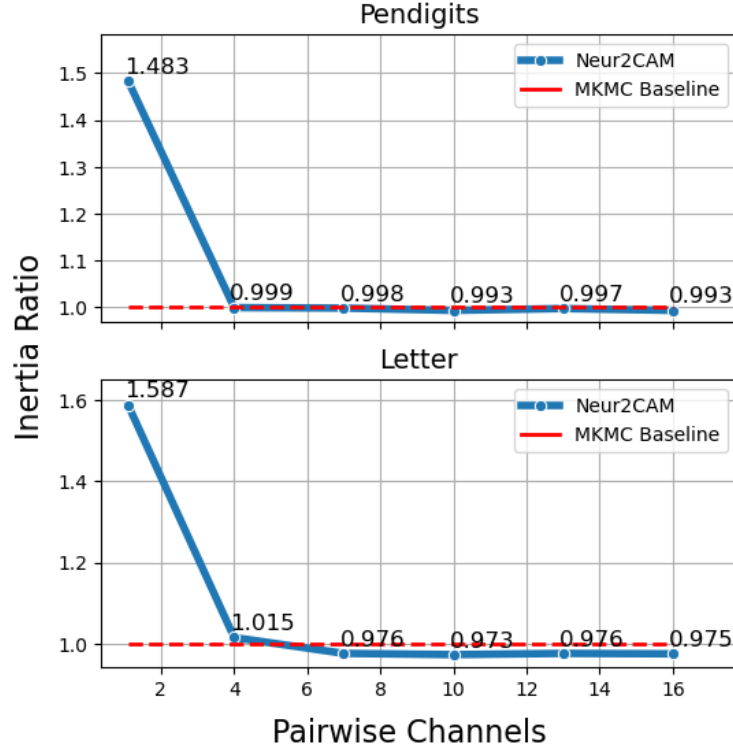


Figure 2: Cost Ratio of Neur2CAM compared to MKMC as more pairwise shape functions are added.

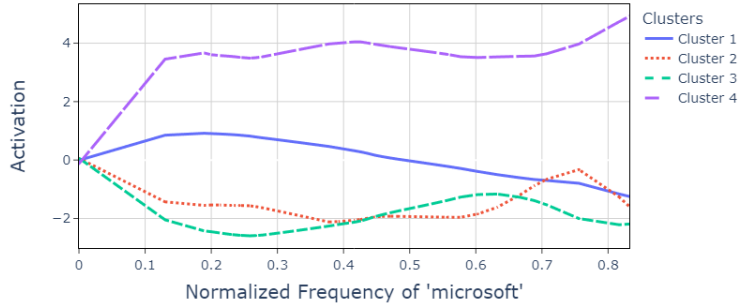


Figure 3: Shape Graphs for "Microsoft" learned when clustering the AG News Dataset

6 Conclusion

In this work, we present NeurCAM, the first approach to interpretable clustering that uses neural GAMs. Our experiments showcase our ability to produce high-quality clusters on tabular data that are comparable to black-box approaches while using a limited number of features and interactions chosen by our proposed selection gate mechanism. We also demonstrate NeurCAM’s ability to utilize deep representations of the data while still providing explanations in a human interpretable feature space on both tabular and text datasets.

NeurCAM is a powerful tool for large-scale clustering tasks for knowledge discovery and can be used as a foundation for further research on interpretable clustering via Generalized Additive Models. Potential extensions of our work involve the joint performance of clustering and representation learning by integrating approaches such as DEC / IEC [Xie et al., 2016, Guo et al., 2017] or VADE [Jiang et al., 2017]. Furthermore, other possible directions include designing specialized GAMs to focus on learned interpretable features from images, such as prototypes [Chen et al., 2019], or time series, such as shapelets [Lines et al., 2012].

References

- Cynthia Rudin. Stop explaining black box machine learning models for high stakes decisions and use interpretable models instead. *Nature machine intelligence*, 1(5):206–215, 2019.
- Haoyu Yang, Lianmeng Jiao, and Quan Pan. A survey on interpretable clustering. In *2021 40th Chinese Control Conference (CCC)*, pages 7384–7388. IEEE, 2021.
- Ali Aouad, Adam N Elmachtoub, Kris J Ferreira, and Ryan McNellis. Market segmentation trees. *M&SOM*, 25(2): 648–667, 2023.
- Kailai Sun, Tianxiang Lan, Yang Miang Goh, Sufiana Safiena, Yueng-Hsiang Huang, Bailey Lytle, and Yimin He. An interpretable clustering approach to safety climate analysis: Examining driver group distinctions. *Accident Analysis & Prevention*, 196:107420, 2024.
- Laura Manduchi, Matthias Hüser, Martin Faltys, Julia Vogt, Gunnar Rätsch, and Vincent Fortuin. T-dpsom: An interpretable clustering method for unsupervised learning of patient health states. In *CHIL*, page 236–245, 2021.
- Rongrong Fu, Weishuai Li, Junxiang Chen, and Mengmeng Han. Recognizing single-trial motor imagery eeg based on interpretable clustering method. *Biomedical Signal Processing and Control*, 63:102171, 2021.
- Dimitris Bertsimas, Agni Orfanoudaki, and Holly Wiberg. Interpretable clustering: an optimization approach. *Machine Learning*, 110:89–138, 2021.
- Ricardo Fraiman, Badih Ghattas, and Marcela Svarc. Interpretable clustering using unsupervised binary trees. *ADAC*, 7: 125–145, 2013.
- Nave Frost, Michal Moshkovitz, and Cyrus Rashtchian. Exkmc: Expanding explainable k -means clustering. *arXiv preprint arXiv:2006.02399*, 2020.
- Magzhan Gabidolla and Miguel Á Carreira-Perpiñán. Optimal interpretable clustering using oblique decision trees. In *KDD*, pages 400–410, 2022.
- Pouya Shati, Eldan Cohen, and Sheila McIlraith. Optimal decision trees for interpretable clustering with constraints. In *IJCAI*, pages 2022–2030, 2023.
- Eldan Cohen. Interpretable clustering via soft clustering trees. In *CPAIOR*, pages 281–298, 2023.
- Sarah Tan, Giles Hooker, Paul Koch, Albert Gordo, and Rich Caruana. Considerations when learning additive explanations for black-box models. *Machine Learning*, pages 1–27, 2023.
- Mitja Luštrek, Matjaž Gams, Sanda Martinčić-Ipšić, et al. What makes classification trees comprehensible? *Expert Systems with Applications*, 62:333–346, 2016.
- Trevor J Hastie. Generalized additive models. In *Statistical models in S*, pages 249–307. Routledge, 2017.
- Tamer Karatekin, Selim Sancak, Gokhan Celik, Sevilay Topcuoglu, Guner Karatekin, Pinar Kirci, and Ali Okatan. Interpretable machine learning in healthcare through generalized additive model with pairwise interactions (ga2m): Predicting severe retinopathy of prematurity. In *Deep Learning and Machine Learning in Emerging Applications*, pages 61–66, 2019.
- Alessia Sarica, Andrea Quattrone, and Aldo Quattrone. Explainable boosting machine for predicting alzheimer’s disease from mri hippocampal subfields. In *BI*, pages 341–350, 2021.
- Rishabh Agarwal, Levi Melnick, Nicholas Frosst, Xuezhou Zhang, Ben Lengerich, Rich Caruana, and Geoffrey E Hinton. Neural additive models: Interpretable machine learning with neural nets. *NeurIPS*, pages 4699–4711, 2021.
- Filip Radenovic, Abhimanyu Dubey, and Dhruv Mahajan. Neural basis models for interpretability. In *NeurIPS*, pages 8414–8426, 2022.
- Chun-Hao Chang, Rich Caruana, and Anna Goldenberg. Node-gam: Neural generalized additive model for interpretable deep learning. In *ICLR*, 2022.
- Shibal Ibrahim, Gabriel Afriat, Kayhan Behdin, and Rahul Mazumder. Grand-slam: Interpretable additive modeling with structural constraints. *Advances in Neural Information Processing Systems*, 36, 2024.
- Cynthia Rudin, Chaofan Chen, Zhi Chen, Haiyang Huang, Lesia Semenova, and Chudi Zhong. Interpretable machine learning: Fundamental principles and 10 grand challenges. *Statistics Surveys*, 16, 2022.
- Ulrike Von Luxburg. A tutorial on spectral clustering. *Statistics and computing*, 17:395–416, 2007.
- Alvin Subakti, Hendri Murfi, and Nora Hariadi. The performance of bert as data representation of text clustering. *Journal of big Data*, 9(1):1–21, 2022.

- Mei-Chih Chang, Peter Bus, and Gerhard Schmitt. Feature extraction and k-means clustering approach to explore important features of urban identity. In *ICMLA*, pages 1139–1144. IEEE, 2017.
- W James Murdoch, Chandan Singh, Karl Kumbier, Reza Abbasi-Asl, and Bin Yu. Definitions, methods, and applications in interpretable machine learning. *National Academy of Sciences*, 116(44):22071–22080, 2019.
- Tessa Han, Suraj Srinivas, and Himabindu Lakkaraju. Which explanation should i choose? a function approximation perspective to characterizing post hoc explanations. In *NeurIPS*, pages 5256–5268, 2022.
- Dylan Slack, Sophie Hilgard, Emily Jia, Sameer Singh, and Himabindu Lakkaraju. Fooling lime and shap: Adversarial attacks on post hoc explanation methods. In *AIES*, pages 180–186, 2020.
- Connor Lawless, Jayant Kalagnanam, Lam M Nguyen, Dzung Phan, and Chandra Reddy. Interpretable clustering via multi-polytope machines. In *AAAI*, pages 7309–7316, 2022.
- Junxiang Chen, Yale Chang, Brian Hobbs, Peter Castaldi, Michael Cho, Edwin Silverman, and Jennifer Dy. Interpretable clustering via discriminative rectangle mixture model. In *IEEE ICDM*, pages 823–828, 2016.
- Jacob Kauffmann, Malte Esders, Lukas Ruff, Grégoire Montavon, Wojciech Samek, and Klaus-Robert Müller. From clustering to cluster explanations via neural networks. *IEEE TNNLS*, 2022.
- Sebastian Bach, Alexander Binder, Grégoire Montavon, Frederick Klauschen, Klaus-Robert Müller, and Wojciech Samek. On pixel-wise explanations for non-linear classifier decisions by layer-wise relevance propagation. *PloS one*, 10(7), 2015.
- Connor Lawless and Oktay Gunluk. Cluster explanation via polyhedral descriptions. In *ICML*, pages 18652–18666, 2023.
- Emilio Carrizosa, Kseniia Kurishchenko, Alfredo Marín, and Dolores Romero Morales. Interpreting clusters via prototype optimization. *Omega*, 107:102543, 2022.
- Renchu Guan, Hao Zhang, Yanchun Liang, Fausto Giunchiglia, Lan Huang, and Xiaoyue Feng. Deep feature-based text clustering and its explanation. *IEEE TKDE*, 34(8):3669–3680, 2020.
- Xi Peng, Yunfan Li, Ivor W Tsang, Hongyuan Zhu, Jiancheng Lv, and Joey Tianyi Zhou. Xai beyond classification: Interpretable neural clustering. *JMLR*, 23(1):227–254, 2022.
- Jonathan Svirsky and Ofir Lindenbaum. Interpretable deep clustering for tabular data. In *Forty-first International Conference on Machine Learning*, 2024.
- Yin Lou, Rich Caruana, Johannes Gehrke, and Giles Hooker. Accurate intelligible models with pairwise interactions. In *KDD*, pages 623–631, 2013a.
- Yin Lou, Rich Caruana, Johannes Gehrke, and Giles Hooker. Accurate intelligible models with pairwise interactions. In *KDD*, pages 623–631, 2013b.
- Chun-Hao Chang, Sarah Tan, Ben Lengerich, Anna Goldenberg, and Rich Caruana. How interpretable and trustworthy are gams? In *KDD*, pages 95–105, 2021.
- Stefan Hegselmann, Thomas Volkert, Hendrik Ohlenburg, Antje Gottschalk, Martin Dugas, and Christian Ertmer. An evaluation of the doctor-interpretability of generalized additive models with interactions. In *MLHC*, pages 46–79, 2020.
- Scott M Lundberg and Su-In Lee. A unified approach to interpreting model predictions. *NeurIPS*, 2017.
- Harmanpreet Kaur, Harsha Nori, Samuel Jenkins, Rich Caruana, Hanna Wallach, and Jennifer Wortman Vaughan. Interpreting interpretability: understanding data scientists’ use of interpretability tools for machine learning. In *CHI*, pages 1–14, 2020.
- Ben Peters, Vlad Niculae, and André FT Martins. Sparse sequence-to-sequence models. In *Proceedings of the 57th Annual Meeting of the Association for Computational Linguistics*, pages 1504–1519, 2019.
- James C Bezdek, Robert Ehrlich, and William Full. Fcm: The fuzzy c-means clustering algorithm. *Computers & geosciences*, 10(2-3):191–203, 1984.
- David Sculley. Web-scale k-means clustering. In *WWW*, pages 1177–1178, 2010.
- William M Rand. Objective criteria for the evaluation of clustering methods. *Journal of the American Statistical association*, 66(336):846–850, 1971.
- Lawrence Hubert and Phipps Arabie. Comparing partitions. *Journal of classification*, 2:193–218, 1985.
- Alexander Strehl and Joydeep Ghosh. Cluster ensembles—a knowledge reuse framework for combining multiple partitions. *JMLR*, 3(Dec):583–617, 2002.

- Junyuan Xie, Ross Girshick, and Ali Farhadi. Unsupervised deep embedding for clustering analysis. In *ICML*, pages 478–487, 2016.
- Adam Paszke, Sam Gross, Francisco Massa, Adam Lerer, James Bradbury, Gregory Chanan, Trevor Killeen, Zeming Lin, Natalia Gimelshein, Luca Antiga, Alban Desmaison, Andreas Kopf, Edward Yang, Zachary DeVito, Martin Raison, Alykhan Tejani, Sasank Chilamkurthy, Benoit Steiner, Lu Fang, Junjie Bai, and Soumith Chintala. PyTorch: An Imperative Style, High-Performance Deep Learning Library. In *NeurIPS*, pages 8024–8035, 2019.
- F. Pedregosa, G. Varoquaux, A. Gramfort, V. Michel, B. Thirion, O. Grisel, M. Blondel, P. Prettenhofer, R. Weiss, V. Dubourg, J. Vanderplas, A. Passos, D. Cournapeau, M. Brucher, M. Perrot, and E. Duchesnay. Scikit-learn: Machine learning in Python. *JMLR*, 12:2825–2830, 2011.
- Diederik P Kingma and Jimmy Ba. Adam: A method for stochastic optimization. *arXiv preprint arXiv:1412.6980*, 2014.
- Benjamin Lengerich, Sarah Tan, Chun-Hao Chang, Giles Hooker, and Rich Caruana. Purifying interaction effects with the functional anova: An efficient algorithm for recovering identifiable additive models. In *AISTATS*, pages 2402–2412, 2020.
- Markelle Kelly, Rachel Longjohn, and Kolby Nottingham. The uci machine learning repository. <https://archive.ics.uci.edu>, 2017.
- Pascal Vincent, Hugo Larochelle, Yoshua Bengio, and Pierre-Antoine Manzagol. Extracting and composing robust features with denoising autoencoders. In *ICML*, pages 1096–1103, 2008.
- Uri Shaham, Kelly Stanton, Henri Li, Boaz Nadler, Ronen Basri, and Yuval Kluger. Spectralnet: Spectral clustering using deep neural networks. In *ICLR*, 2018.
- Xiang Zhang, Junbo Zhao, and Yann LeCun. Character-level convolutional networks for text classification. *NeurIPS*, 2015.
- Sören Auer, Christian Bizer, Georgi Kobilarov, Jens Lehmann, Richard Cyganiak, and Zachary Ives. Dbpedia: A nucleus for a web of open data. In *ISWC*, pages 722–735, 2007.
- Ken Lang. Newsweeder: Learning to filter netnews. In *ICML*, pages 331–339, 1995.
- Zhiguo Wang, Haitao Mi, and Abraham Ittycheriah. Semi-supervised clustering for short text via deep representation learning. In *CoNLL*, 2016.
- George A Miller. Wordnet: a lexical database for english. *Communications of the ACM*, 38(11):39–41, 1995.
- Steven Bird, Ewan Klein, and Edward Loper. *Natural language processing with Python: analyzing text with the natural language toolkit*. "O'Reilly Media, Inc.", 2009.
- Kaitao Song, Xu Tan, Tao Qin, Jianfeng Lu, and Tie-Yan Liu. MpNet: Masked and permuted pre-training for language understanding. *NeurIPS*, pages 16857–16867, 2020.
- Nils Reimers and Iryna Gurevych. Sentence-bert: Sentence embeddings using siamese bert-networks. In *EMNLP*, 11 2019.
- Xifeng Guo, Long Gao, Xinwang Liu, and Jianping Yin. Improved deep embedded clustering with local structure preservation. In *IJCAI*, pages 1753–1759, 2017.
- Zhuxi Jiang, Yin Zheng, Huachun Tan, Bangsheng Tang, and Hanning Zhou. Variational deep embedding: an unsupervised and generative approach to clustering. In *IJCAI*, pages 1965–1972, 2017.
- Chaofan Chen, Oscar Li, Daniel Tao, Alina Barnett, Cynthia Rudin, and Jonathan K Su. This looks like that: deep learning for interpretable image recognition. In *NeurIPS*, 2019.
- Jason Lines, Luke M Davis, Jon Hills, and Anthony Bagnall. A shapelet transform for time series classification. In *KDD*, pages 289–297, 2012.
- Stuart Lloyd. Least squares quantization in pcm. *IEEE transactions on information theory*, 28(2):129–137, 1982.

A Official Implementation

The official implementation for our approach can be accessed at <https://github.com/optimal-uoft/NeurCAM>.

B Dataset Information

Table 4: Tabular Datasets

Dataset	N	D	K
Adult	48,842	105	2
Avila	20,867	10	12
Gas Drift	13,910	128	6
Letters	20,000	16	26
Pendigits	10,992	16	10
Shuttle	58,000	9	7

Table 5: Text Datasets

Dataset	N	D	K
AG News	4,000	338	4
DBPedia	14,000	351	14
20 Newsgroups	18,846	1,065	20
Yahoo	10,000	474	10

B.1 Tabular Representation Details

Our SpectralNet [Shaham et al., 2018] configuration is as follows:

- Spectral Net Hidden Dimensions: [512, 512, 2048, K]
- Siamese Net Hidden Dimensions: [512, 512, 2048, K]

All other parameters are the default presented by the original authors [Shaham et al., 2018].

Our DAE Configuration Configuration is as follows:

- Hidden Dimensions: [128, 64, 32, 16] (Reversed on for the decoder).
- Bottleneck Dimension: 8
- Input Dropout Probability: 0.1

The DAE is trained using the same configuration as NeurCAM.

B.1.1 Text Representation Details

To create our interpretable representation, we first remove the punctuation from all the datapoints and then tokenize then. We then lowercase all tokens and remove English stopwords. Then we lemmatize all words using the WordNet [Miller, 1995] lemmatizer available in the Natural Language Toolkit (NLTK) [Bird et al., 2009]. Additionally, we remove corpus-specific stopwords that appear in more than 99% of the datapoints and rare words that appear in less than 1% of the documents. Finally we then calculate term frequency in each datapoint and normalize the representation such that the L_2 norm of the resultant vector is equal to 1.0.

For our contextual representation, we utilize embeddings from the MPNet transformer available in the Sentence Transformers package [Reimers and Gurevych, 2019]. This model has a representation size of 768, a maximum sequence length of 384, and uses mean pooling to construct its embedding. More details about this model can be found at .

C Training and Implementation Details

NeurCAM is trained using Adam [Kingma and Ba, 2014] for 1000 epochs and the learning rate is halved when the loss plateaus for 100 epochs. The selection gate tempering starts after 400 warmup epochs and continues for 100 epochs. For Neur2CAM, the pairwise gate temperature parameter T_2 is fully tempered before tempering T . To adjust for this additional tempering time, we allow Neur2CAM to also train for an extra 100 epochs as well.

To train the SCT, we follow Cohen [2023] and opt to use the RMSProp optimizer for 1000 epochs with a cyclic scheduler. After the initial round of training, we slowly ramp the sparsity regularization weight by .001 every training step and terminate the training when each node of the tree utilizes only one feature [Cohen, 2023].

For Mini-Batch K -Means, we set the number of points used for initialization to five times the batch size and performed five initializations.

While the axis-aligned TAO described by Gabidolla and Carreira-Perpiñán [2022] initializes their tree via ExKMC [Frost et al., 2020], we instead initialize the tree via a CART decision tree fit on the results of K -Means [Lloyd, 1982] clustering as ExKMC does not support OSM on disentangled representations. TAO was run for 50 iterations.

Table 6: Hyperparameter details for all approaches and baselines.

	NeurCAM	Neur2CAM	SCT	TAO	Mkmc
Batch Size	512	512	512	—	512
LR	0.002	0.002	0.002	—	—
Optimizer	Adam	Adam	RMSProp	—	—
LR Scheduler	Plateau ⁽¹⁾	Plateau ⁽¹⁾	Cyclic ⁽²⁾	—	—
Hidden Dim.	256	256	—	—	—
N. Hidden	2	2	—	—	—
Activation	ReLU	ReLU	—	—	—
Warmup Steps	400	400	—	—	—
T Tempering Steps	100	100	—	—	—
T_2 Tempering Steps	—	100	—	—	—
Total Epochs	1000	1100	1000	50	1000
B	64	64	—	—	—
Branching Reg. Weight	—	—	0.1	—	—
Sparsity Reg. Weight	—	—	0.001	—	—
γ	1	1	—	—	—
m	1.05 or 1.025 ⁽³⁾	1.05 or 1.025 ⁽³⁾	1.05 or 1.025 ⁽³⁾	—	—

(1) Halve learning rate when the loss does not improve for 100 epochs. (2) Cycled between 0.002 and 0.00002 every 100 epochs. (3) After the end of the main training epochs, this parameter is increased by 0.001 every training step until every node is fully sparse. For more information, we refer readers to Cohen [2023]. (3) For tabular we use $m = 1.05$, for text we use $m = 1.025$. We empirically observed that a higher m for text datasets resulted in a degenerate solution, therefore a smaller m value was used.

D Full Tabular Results

Table 7: Results from our tabular clustering experiments. The best overall results are highlighted in bold, while the best interpretable results are underlined. The dashed line separates interpretable and non-interpretable approaches.

		ARI		NMI		ACC		Iner.	
		AE	Spectral	AE	Spectral	AE	Spectral	AE	Spectral
Adult	NCAM	-0.018	0.000	0.002	0.000	0.720	0.761	4.245	0.994
	N2CAM	-0.026	0.000	0.004	0.000	0.711	0.761	4.245	0.994
	TAO-5	-0.006	0.002	0.000	0.000	0.738	<u>0.578</u>	<u>5.531</u>	0.698
	TAO-7	-0.008	-0.001	0.001	0.000	0.735	0.505	5.235	0.564
	SCT-5	-0.007	0.043	0.000	0.006	0.737	0.685	4.772	<u>0.837</u>
	SCT-7	-0.007	0.043	0.000	0.009	0.736	0.648	4.497	0.781
	mKMC	-0.013	-0.001	0.001	0.000	0.728	0.580	4.062	0.121
Avila	NCAM	0.051	0.070	0.136	0.181	0.324	0.268	2.045	3.110
	N2CAM	0.069	0.072	0.143	0.176	0.338	0.269	1.952	2.736
	TAO-5	0.063	0.046	0.153	0.135	<u>0.335</u>	0.258	2.450	<u>5.538</u>
	TAO-7	0.056	0.067	0.133	0.165	0.327	0.273	1.281	3.706
	SCT-5	0.068	0.089	0.131	0.193	0.297	0.322	<u>3.136</u>	6.630
	SCT-7	0.015	<u>0.052</u>	0.094	<u>0.137</u>	0.254	0.263	2.941	6.110
	mKMC	0.073	0.072	0.157	0.176	0.337	0.268	1.782	2.686
GasDrift	NCAM	0.068	0.120	0.247	0.259	0.363	0.407	2.502	1.617
	N2CAM	0.041	0.183	0.199	0.326	0.330	0.447	3.216	2.493
	TAO-5	0.065	<u>0.162</u>	0.241	<u>0.266</u>	0.357	<u>0.427</u>	2.187	1.852
	TAO-7	0.062	0.164	0.236	0.278	0.355	0.430	1.877	1.552
	SCT-5	0.124	0.069	0.255	0.198	0.391	0.332	<u>3.462</u>	2.169
	SCT-7	0.109	0.078	0.235	0.197	0.393	0.365	<u>3.346</u>	1.977
	mKMC	0.100	0.167	0.226	0.285	0.355	0.432	2.858	1.477
Letter	NCAM	0.151	0.242	0.373	0.545	0.260	0.402	1.844	5.154
	N2CAM	0.173	<u>0.242</u>	0.402	<u>0.540</u>	0.299	0.406	1.624	4.702
	TAO-5	0.115	<u>0.161</u>	0.343	0.418	0.241	0.331	2.612	<u>15.332</u>
	TAO-7	0.139	0.192	0.375	0.475	0.271	0.382	1.953	8.104
	SCT-5	0.139	0.171	0.344	0.383	0.240	0.281	3.114	18.116
	SCT-7	0.128	0.146	0.326	0.384	0.242	0.294	3.046	15.125
	mKMC	0.156	0.256	0.384	0.551	0.286	0.418	1.403	3.697
Pendigits	NCAM	0.506	0.754	0.629	0.822	0.698	0.871	1.344	0.712
	N2CAM	0.502	0.757	0.643	0.826	0.653	0.872	<u>1.355</u>	0.648
	TAO-5	0.481	0.692	0.607	0.770	0.681	0.841	1.610	1.196
	TAO-7	0.493	0.743	0.626	0.817	0.693	0.867	1.406	0.762
	SCT-5	0.402	0.520	0.548	0.636	0.550	0.730	1.954	3.052
	SCT-7	0.458	0.670	0.597	0.732	0.646	0.824	1.790	1.716
	mKMC	0.489	0.754	0.624	0.831	0.677	0.872	1.330	0.611
Shuttle	NCAM	0.392	0.380	0.428	0.500	0.778	0.654	3.072	0.383
	N2CAM	0.382	0.376	0.377	0.494	0.771	0.653	2.002	0.390
	TAO-5	0.393	0.376	0.378	0.493	0.775	0.653	3.367	0.470
	TAO-7	0.394	0.375	0.377	0.493	0.775	0.652	2.135	0.412
	SCT-5	<u>0.230</u>	0.245	0.376	0.465	0.494	0.521	4.871	1.955
	SCT-7	0.239	0.199	0.349	0.429	0.544	0.461	4.875	0.946
	mKMC	0.460	0.249	0.411	0.435	0.691	0.549	4.655	0.881
Average	NCAM	0.192	0.261	0.303	0.385	0.524	0.561	2.509	1.995
	N2CAM	0.190	0.272	0.295	0.394	0.517	0.568	2.399	1.994
	TAO-5	0.185	0.240	0.287	0.347	0.521	0.515	2.960	4.181
	TAO-7	0.189	0.257	0.291	0.371	0.526	0.518	2.315	2.517
	SCT-5	0.159	0.190	0.276	0.314	0.452	0.479	<u>3.552</u>	5.460
	SCT-7	0.157	0.198	0.267	0.315	0.469	0.476	3.416	4.443
	mKMC	0.211	0.250	0.301	0.380	0.512	0.520	2.682	1.579

E Full Text Results

Table 8: Results from our text clustering experiments. The best overall results are highlighted in bold, while the best interpretable results are underlined. The dashed line separates interpretable and non-interpretable approaches.

		ARI \uparrow	NMI \uparrow	ACC \uparrow	Iner. \downarrow
AG News	NCAM	0.464	0.462	0.755	728.099
	N2CAM	0.609	0.576	0.828	720.732
	TAO-5	0.035	0.163	0.405	751.176
	TAO-7	0.075	0.181	0.471	750.871
	SCT-5	0.209	0.288	0.562	742.914
	SCT-7	0.252	0.282	0.563	742.650
	mKMC	0.538	0.548	0.762	719.803
DBPedia	NCAM	0.636	0.761	0.770	640.994
	N2CAM	0.676	0.802	0.738	638.379
	TAO-5	0.152	0.512	0.375	697.140
	TAO-7	0.218	0.561	0.471	681.172
	SCT-5	0.286	0.564	0.514	690.059
	SCT-7	0.262	0.546	0.452	688.185
	mKMC	0.774	0.842	0.845	627.486
Newsgroups	NCAM	0.185	0.388	0.404	682.520
	N2CAM	0.296	0.477	0.471	661.685
	TAO-5	0.012	0.169	0.161	744.979
	TAO-7	0.013	0.215	0.203	735.034
	SCT-5	0.006	0.053	0.099	759.167
	SCT-7	0.013	0.051	0.121	756.019
	mKMC	0.400	0.561	0.550	630.874
Yahoo	NCAM	0.150	0.240	0.407	735.257
	N2CAM	0.240	0.329	0.465	724.446
	TAO-5	0.012	0.099	0.201	756.741
	TAO-7	0.018	0.132	0.239	754.356
	SCT-5	0.009	0.027	0.156	762.317
	SCT-7	0.008	0.019	0.143	764.162
	mKMC	0.251	0.328	0.480	718.121
Average	NCAM	0.359	0.463	0.584	696.717
	N2CAM	0.455	0.546	0.625	686.311
	TAO-5	0.052	0.236	0.286	737.509
	TAO-7	0.081	0.272	0.346	730.358
	SCT-5	0.127	0.233	0.333	738.614
	SCT-7	0.134	0.224	0.320	737.754
	mKMC	0.491	0.570	0.659	674.071

F NeurCAM Explanation Consistency

NeurCAM allows users to limit the number of features used to build clusters by setting the number of shape functions NeurCAM learns to a small number. To evaluate the consistency of the selection mechanism across different runs of the algorithm, we report the selected features shared across different runs of NeurCAM on our text datasets. As NeurCAM may converge to a locally optimum solution, we perform multiple runs and select the runs with the lowest Inertia values for the hard clustering, similar to the evaluation setting of our tabular and text clustering experiment. For this set of experiments, we run fifteen random seeds and choose the five runs with the lowest Inertia values for the hard clustering. We then select the top K features according to importance. Finally, we calculate the average intersection of the top K words between each pair of runs for different K values. The results of this analysis can be seen in Table 9. In addition, we provide the top ten important words for the runs for each dataset in Tables 10, 11, 12, and 13. We observe that the runs share a significant intersection in the top- K features with more than a 50% average intersection across all the various K values.

Table 9: Average number of shared important terms across pairs of runs.

Dataset	Average Intersection Size @ K				
	$K = 10$	$K = 25$	$K = 50$	$K = 75$	$K = 100$
AG News	5.3	16.8	29.7	43.3	55.6
DBPedia	8.4	19.3	36.8	49.5	62.4
Newsgroups	5.5	14.9	29.1	40.9	55.1
Yahoo	5.9	14.3	32.5	45.7	55.8

AG News				
company	iraq	company	company	company
iraq	company	39s	iraq	price
corp	corp	iraq	microsoft	corp
game	microsoft	computer	internet	technology
player	internet	microsoft	market	game
new	oil	game	oil	iraq
market	team	oil	team	night
microsoft	new	software	player	microsoft
software	price	corp	victory	internet
sunday	season	market	president	billion

Table 10: Top 10 Important words for five different runs of NeurCAM for the AG News dataset.

DBPedia				
born	born	born	born	specie
located	specie	located	specie	born
built	located	film	film	film
specie	genus	built	located	located
film	district	school	county	district
album	family	genus	village	village
village	film	district	school	school
district	village	specie	built	family
released	school	family	district	genus
school	built	released	album	built

Table 11: Top 10 Important words for five different runs of NeurCAM for the DBPedia dataset.

Newsgroups				
game	window	window	window	people
work	government	car	know	window
team	people	people	team	car
government	car	game	car	god
car	god	program	card	christian
year	program	government	government	government
im	problem	software	drive	drive
window	software	god	christian	game
problem	card	thanks	driver	price
drive	game	team	space	software

Table 12: Top 10 Important words for five different runs of NeurCAM for the 20Newsgroups dataset.

Yahoo				
help	help	help	think	think
think	people	people	guy	girl
song	think	god	help	people
people	girl	girl	girl	god
girl	god	guy	dont	guy
guy	guy	want	people	dont
love	want	computer	world	love
god	world	problem	woman	year
know	love	jesus	computer	problem
computer	know	religion	american	friend

Table 13: Top 10 Important words for five different runs of NeurCAM for the Yahoo dataset.

G NeurCAM Time Analysis

In Table 14, we provide the runtime of NeurCAM and Neur2CAM on the text dataset. This set of experiments was run on a Nvidia GEFORCE 3080 RTX with 10GB VRAM, 32GB RAM, and a 12th Gen Intel(R) Core(TM) i7-12700 @ 2.10 GHz. All results are across five seeds. Note that we do not report the runtime of TAO as this approach is not trained using scalable mini-batch methods, making the performance of TAO incomparable to the runtime of NeurCAM and the SCT. Additionally, Minbatch K -Means (a uninterpretable clustering model) is omitted from the table as it is used to initialize the centroids for our model, making the initialization time of NeurCAM equivalent to the time required to run Minibatch K -Means.

Table 14: Average Training time in seconds.				
		Initialization	Warmup	Total
AGNews	NCAM	0.05	168.72	426.45
	N2CAM	0.06	312.26	873.13
	SCT-7	—	—	1001.45
DBPedia	NCAM	0.19	515.85	1308.47
	N2CAM	0.19	961.75	2674.51
	SCT-7	—	—	2353.12
Newsgroups	NCAM	0.30	664.77	1696.48
	N2CAM	0.30	1261.56	3508.65
	SCT-7	—	—	3032.01
Yahoo	NCAM	0.10	368.99	935.36
	N2CAM	0.10	708.54	1966.50
	SCT-7	—	—	1401.55

Table 15: Standard Deviation of Training Time in seconds.

		Initialization	Warmup	Total
AGNews	NCAM	0.02	5.19	2.83
	N2CAM	0.01	3.93	6.73
	SCT	—	—	119.15
DBPedia	NCAM	0.02	5.17	3.60
	N2CAM	0.03	3.69	12.00
	SCT	—	—	32.70
Newsgroups	NCAM	0.03	10.41	13.38
	N2CAM	0.03	7.87	21.77
	SCT	—	—	21.65
Yahoo	NCAM	0.01	2.72	6.68
	N2CAM	0.01	4.42	5.67
	SCT	—	—	13.51

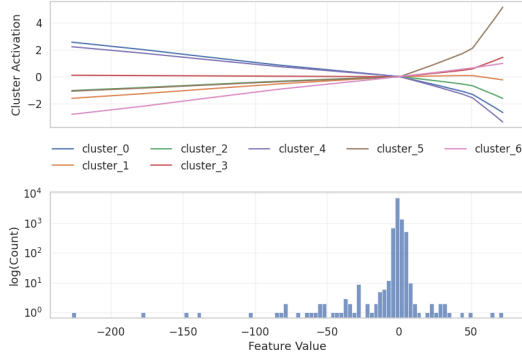
H Interpretability Example

The interpretability of NeurCAM comes from the fact that the learned shape functions for each feature and interaction can be visualized and summarized, allowing stakeholders to understand the impact individual features have on the end prediction. In this section, we demonstrate this capability on the Shuttle dataset and provide visualizations of the explanations from NeurCAM. The Shuttle dataset contains 9 numerical attributes and the full information on the dataset can be found at the following link: <https://archive.ics.uci.edu/dataset/148/statlog+shuttle>.

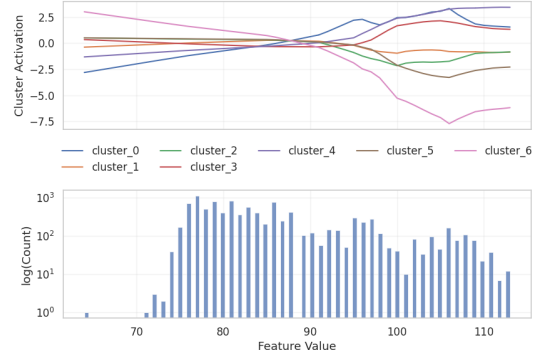
For this, set of experiments, we allow for nine single-feature selection shape functions and one pairwise gate. Our interpretable representation is the original feature space and the representation used by the loss function are deep embeddings from a pre-trained Denoising AutoEncoder. This model achieved an ARI of 0.485, an NMI of 0.424, an ACC of 0.738, and an Inertia of 2.88.

Single Feature Shape Graphs: We first plot the single-feature shape graphs for NeurCAM along with the distribution of values of the features (Figure 4). Note that while we allowed at most nine features, NeurCAM only selected seven features. Examining these shape graphs, we observe some interesting behaviors. For example, we observe that feature A3 (Figure 4b) seems to be important in determining whether or not a point is in cluster 6, as when the value of A3 is high, NeurCAM reduces the weight assigned to cluster 6, but increases it slightly when the value of A3 is low. Another observed pattern is that when the value of feature A7 (Figure 4e) is high (above 60), NeurCAM assigns a high weight to cluster 4 and 6, but significantly reduces the weight to cluster 0.

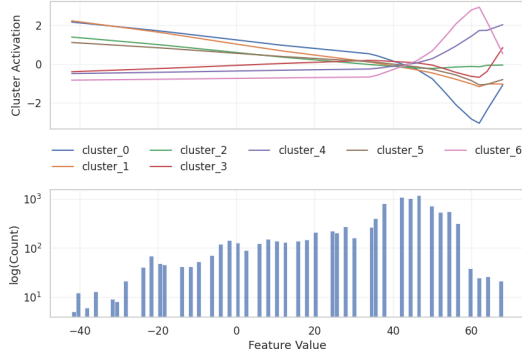
Pairwise Shape Graphs: The pairwise interactions of a GA²M can be visualized as a set of heatmaps, and we plot the pairwise shape graph learned by NeurCAM in Figure 5 following the format utilized by Chang et al. [2022]. Examining these shape graphs, we can see some interesting patterns. For example, when A3 is approximately equal to 90 and A9 is approximately equal to 20, NeurCAM assigns more weight to clusters 0 (Figure 5a), 3 (Figure 5d), and 4 (Figure 5e) while reducing the weights assigned to cluster 5 (Figure 5f).



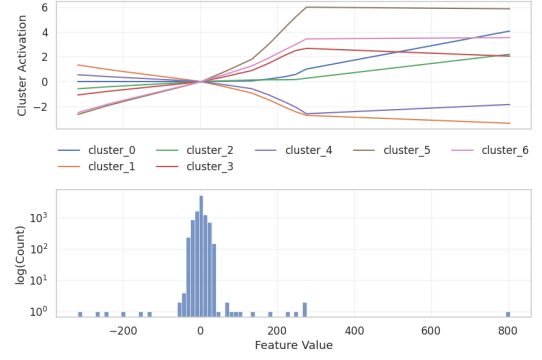
(a) Feature A2



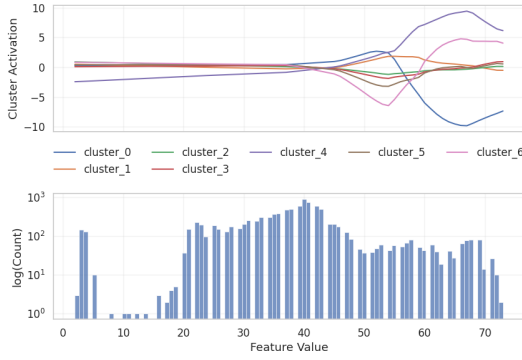
(b) Feature A3



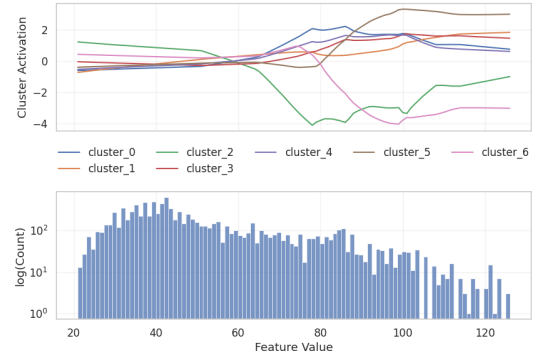
(c) Feature A5



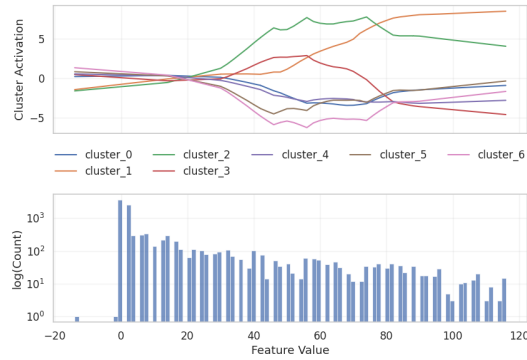
(d) Feature A6



(e) Feature A7

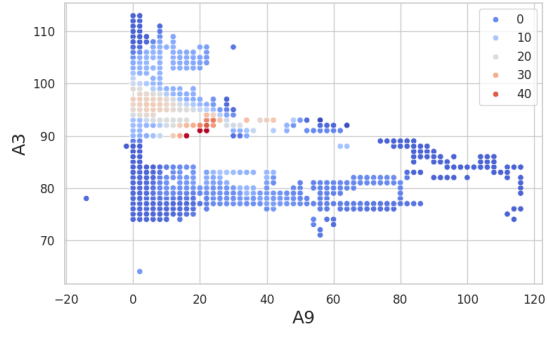


(f) Feature A8

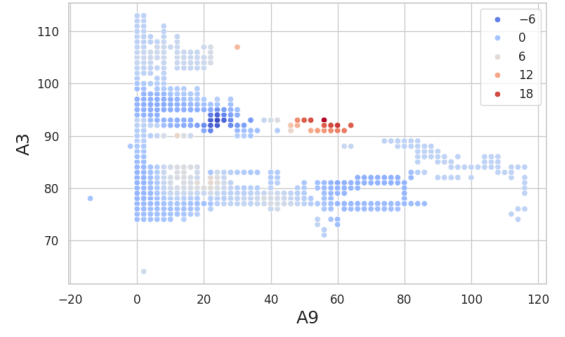


(g) Feature A9

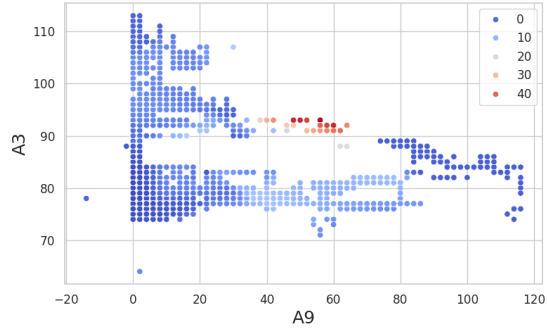
Figure 4: Single Feature Shape Graphs for the Shuttle Dataset (Top) as well as feature value histograms (bottom)



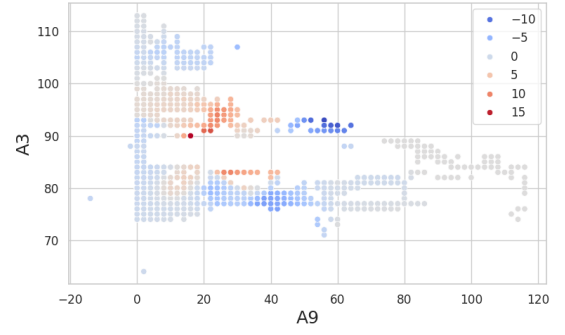
(a) Cluster 0



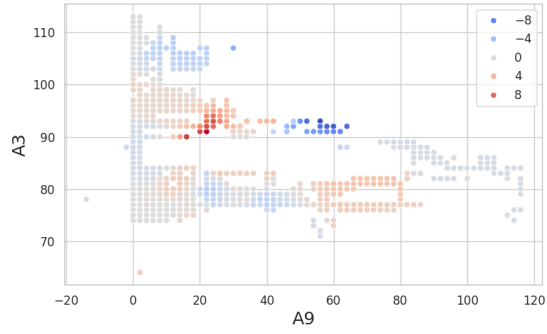
(b) Cluster 1



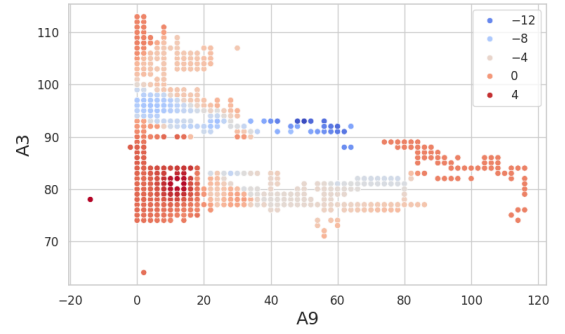
(c) Cluster 2



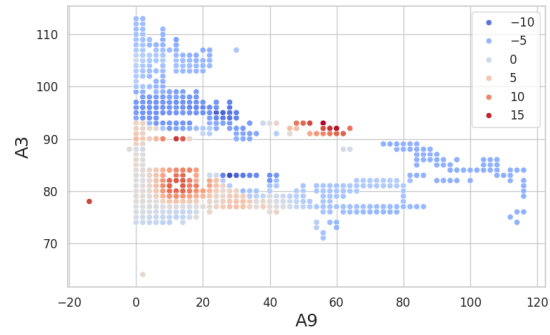
(d) Cluster 3



(e) Cluster 4



(f) Cluster 5



(g) Cluster 6

Figure 5: Pairwise Feature Shape Graph for the Shuttle Dataset